Cu-doped bioactive glass with enhanced in vitro bioactivity and antibacterial properties

Ceramics International 50 (2024) 5091–5103

Contents lists available at ScienceDirect

Ceramics International

journal homepage: www.elsevier.com/locate/ceramint

Cu-doped bioactive glass with enhanced *in vitro* bioactivity and antibacterial properties

Mari Lallukka [a], Marta Miola [a], Ziba Najmi [b], Andrea Cochis [b], Silvia Spriano [a], Lia Rimondini [b,**], Enrica Verné [a,*]

[a] Department of Applied Science and Technology, Politecnico di Torino, Corso Duca degli Abruzzi 24, 10129, Torino, Italy
[b] Department of Health Sciences, Center for Translational Research on Autoimmune and Allergic Diseases—CAAD, Università Del Piemonte Orientale UPO, Corso Trieste 15/A, 28100, Novara, Italy

ARTICLE INFO

Handling Editor: Dr P. Vincenzini

Keywords:
Bioactive glass
Copper
Ion exchange
Antibacterial

ABSTRACT

This work aimed to optimize, produce and characterize Cu-doped bioactive glasses which are antibacterial without the addition of antibiotics obtained via ion exchange in an aqueous solution. According to morphological, compositional and structural analyses, 0.001 M was selected as the most optimal concentration of the ion exchange solution. The doped glass was then compared to the undoped one to investigate the effect of Cu-doping on the glass surface composition and bioactivity. Cu-doping was found to enhance the bioactivity kinetics and the following hydroxyapatite formation, evidenced by X-ray diffraction, energy dispersive X-ray spectroscopy, and zeta potential measurements. Besides that, the zeta potential titration measurements confirmed that the Cu-doping did not alter the surface chemical stability of the glass both in the inflammatory and physiological pH range. Moreover, the leaching ability of Cu^{2+}-ions, both in physiological and inflammatory-mimicking conditions, was measured, followed by an in-depth study of the antibacterial properties, using two protocols to distinguish between the antiadhesive, antibacterial, and antibiofilm effects. For both protocols, a reduction of metabolic activity and Colony-Forming Unit after 24 h against *Staphylococcus aureus* Multi-Drug resistance strain was evidenced. These results showed that Cu-doped glass could show potential as a bioactive and antibacterial surface for bone surgery applications.

1. Introduction

Bioactive glasses (BAGs) are a group of ceramic biomaterials used especially for bone regeneration applications owing to their inherent bioactivity, which can be defined as the ability to develop a direct and strong bond to tissues as a consequence of subsequent chemical reactions [1]. In addition to bioactivity and stimulating effects on bone formation, BAGs' potential as antibacterial materials is another interesting aspect. BAGs are known to have antibacterial activity even without the addition of ions or drugs into the composition. This is due to the local pH increase resulting from the exchange of glass network-modifier ions with H^+ -ions from the surrounding fluids, an increase in the osmotic pressure, and the presence of released BAG debris [2,3]. However, this inherent bactericidal ability can be significantly improved by doping BAGs with antibacterial metal ions, such as copper, silver, zinc, and strontium [4].

Therapeutic metal ions can be defined as ions that can bring additional biological properties to the BAGs, such as antibacterial performance, improved osteogenesis, and anti-inflammatory properties [4]. Copper (Cu) is one of the most studied metallic elements for biomedical use [5]. For instance, Cu has been found to possess antimicrobial properties both towards Gram-positive and Gram-negative bacteria [6] through disruption of the bacterial cell membrane integrity, production of Reactive Oxygen Species (ROS), and degradation of the DNA [7–9]. The antibacterial effect of the leaching Cu^{2+}-ions is dose-dependent, meaning that the antibacterial effect is improved with increasing ion concentration. However, from the glass composition's perspective, adding a high amount of Cu to the glass as a modifier ion can affect glass solubility and bioactivity [5].

In addition to antibacterial properties, the BAG doping with Cu can be beneficial from the perspective of tissue regeneration: the presence of Cu is known to promote angiogenesis, or in other words, of new blood

* Corresponding author.
** Corresponding author.
E-mail addresses: lia.rimondini@uniupo.it (L. Rimondini), enrica.verne@polito.it (E. Verné).

https://doi.org/10.1016/j.ceramint.2023.11.253
Received 24 October 2023; Received in revised form 14 November 2023; Accepted 20 November 2023
Available online 22 November 2023

vessel formation, through stimulation of endothelial cells [10,11], human umbilical vein endothelial cells (HUVECs) [12], and through an effect on Hypoxia-Inducible Factor-1 (HIF-1) [13], leading to activation of Vascular Endothelial Growth Factor (VEGF) [14] leading to angiogenesis [15]. However, Cu is cytotoxic and pro-inflammatory in high concentrations, especially in the case of nanoparticles [16], so understanding and controlling the release profile of leaching Cu is essential.

Cu has been incorporated into BAGs in the form of oxide as a network modifier, ions, or nanoparticles. Most commonly the sol-gel process has been implemented to produce Cu-doped BAGs, for example as a form of electrospun fibers [17], nanoparticles (NPs) [18], or powders [19]. In the case of melt-derived glasses, Cu has been introduced to silicate [20], phosphate [21,22], and borate [23] glasses. In addition, different composites have been prepared, such as a composite coating including mesoporous BAG (MBG) NPs with various amounts of added Cu and chitosan by electrophoretic deposition [24], Cu-doped MBGNPs in a nanocomposite bioink also containing oxidized alginate or gelatin [25], Cu-doped silicate glass as a filler for Poly(methyl methacrylate)-based bone cement [26], and zein-BAG/Cu coatings [27].

In terms of surface doping without affecting the glass bulk properties, the ion-exchange process has been performed traditionally in molten salts [28–30]. However, ion exchange has also been performed in an aqueous solution where lower reaction temperatures can be used. For instance, Miola et al. implemented an ion exchange process for melt-derived BAG in powder form in an aqueous solution of Cu(II) acetate. They showed the incorporation of Cu^{2+} to the BAG as ionic species and Cu^{2+} salts precipitates without the introduction of crystalline phases or negative effect on the glass bioactivity. Finally, the antibacterial properties of the Cu-doped glass were demonstrated towards *Staphylococcus aureus* and *Staphylococcus epidermidis*, showing the potential for antibacterial applications [26,31,32].

In the present work, the aim was to produce bulk melt-derived silica glasses, doped with ionic Cu^{2+}, to combine bioactivity with antibacterial properties. This was done by implementing the previously studied ion-exchange protocol for glass powders [31] to bulk glasses in aqueous Cu(II) acetate solution, and optimizing it to create a Cu^{2+}-rich surface without affecting the glass amorphous nature, morphology, or bioactivity. In addition, the zeta potential of the Cu-doped surface, and the leaching of the Cu^{2+}-ions were studied both in physiological and inflammatory pH conditions. Finally, the biological properties of the Cu-doped bioactive glasses were compared to undoped specimens according to two different protocols: i) International Standard Organization (ISO22196) for antibacterial evaluation and ii) UPO protocol that was previously validated by the Authors for antiadhesive and antibiofilm assessment [33], towards Gram-positive pathogen, *Staphylococcus aureus* Multi-Drug resistance (MDR) strain.

2. Materials and methods

2.1. Sample preparation

A silica-based bioactive glass, SBA3 ($48SiO_2$–$26Na_2O$–$22CaO$–$3P_2O_5$–$0.43B_2O_3$–$0.57Al_2O_3$, in mol.%) was prepared using the melt and quenching technique in the bar form. SBA3 as a powder form has been previously doped successfully with Cu^{2+}-ions by ion exchange [31], and therefore, it is of interest to here further study the Cu-doping of SBA3 as a bulk surface.

For SBA3, the glass precursors (SiO_2, Na_2CO_3, $Ca_3(PO_4)_2$, $CaCO_3$, H_3BO_3, Al_2O_3, Sigma Aldrich, Switzerland, reagent grade >99%) were mixed and then melted in a platinum crucible at 1450 °C for 1 h, poured into a pre-heated cylindrical brass mold (Ø = 10 mm) to obtain bars, and then annealed at 500 °C for 13 h. The glass bar was let to slowly cool to room temperature overnight after annealing. The bars were cut into discs of 10 mm diameter and 2 mm thickness (Buehler IsoMet High Speed Pro), which were then polished (Struers LaboPol-2) with SiC abrasive papers ranging from 320 to 1200 grit to level the surfaces.

2.1.1. Ion exchange

The sample discs cut from the glass bars then went through ion exchange in an aqueous solution to incorporate Cu^{2+} ions on the samples' surface. The previously published protocol for Cu^{2+}-ion exchange for glass in the powder form [31] was used as a starting point to find optimized process conditions for bulk glass. According to that, the discs were soaked in Cu(II)acetate ($Cu(CH_3COO)_2{\cdot}H_2O$, Sigma Aldrich, Switzerland) solution at different concentrations (0.05 M, 0.01 M, and 0.001 M) for 1 h at 37 °C. After the process, the samples were rinsed with bi-distilled water and dried at room temperature overnight.

2.2. Sample physicochemical characterization

2.2.1. Field emission scanning electron microscopy (FESEM)

Field emission scanning electron microscopy (FESEM) equipped with Energy-dispersive X-ray spectroscopy (EDS) (SupraTM 40, Zeiss) was performed on all the samples in triplicates to assess their morphology and composition. Samples were mounted on double-sided carbon tape and coated with platinum.

2.2.2. X-ray diffraction (XRD)

The SBA3 and Cu-SBA3 sample discs were characterized in terms of their phase composition by X-ray diffraction (XRD, Malvern PANalytical X'Pert PRO diffractometer), using the Bragg-Brentano camera geometry and the Cu Kα incident radiation. The 2θ range used for sample measurements was from 10° to 70°. The data from the obtained spectra were further analyzed by using the X-Pert HighScore Software and PCPDF database.

2.2.3. In-vitro bioactivity testing and Cu^{2+}-ion release in simulated body fluid (SBF) and pH5 sodium acetate buffer

The glass samples of SBA3 and Cu-SBA3 were subjected to *in vitro* bioactivity tests by soaking them in simulated body fluid (SBF). The SBF was prepared using the protocol developed by Kokubo et al. [34]. In addition to soaking samples in SBF, a sodium acetate/acetic acid (HAc/NaAc) buffer was implemented as a second soaking solution to mimic Cu^{2+}-release in inflammatory-mimicking low pH conditions, occurring in infections [35,36]. The HAc/NaAc buffer was prepared at the concentration of 0.1 M and pH was adjusted to 5 by adding 1 M NaOH.

Polished glass discs were immersed in 50 mL of SBF for fixed periods (1, 3, 7, 14, and 28 days), with five replicate samples of each glass per time point. Samples were maintained at 37 °C in an incubating shaker with an orbital speed of 120 rpm to simulate the physiological fluid flow.

The change in the solution pH was recorded for each immersion time by pH meter (Hanna Edge HI2020, accuracy ± 0.01) and compared to a blank sample containing only SBF. Then samples were rinsed carefully with bi-distilled water and let to dry at room temperature.

Both solutions at each time point were collected and the cumulative ion release for each sample was calculated by adding the ion release value at the selected time point to the previous ones. The cumulative curves were obtained by using the average of each sample. The Cu^{2+}-ion release was determined by an inductively coupled plasma mass spectrometer (ICP-MS, iCAPTM Q, Thermo Fisher Scientific).

2.2.4. Zeta potential titration

The measurements were performed both on as-prepared glasses and SBF-soaked ones to measure the surface zeta potential as a function of pH and the isoelectric point utilizing the streaming potential technique. The used instrument was an electrokinetic analyzer for solid surfaces (SurPASS, Anton Paar, Austria). An aqueous solution of KCl (0.001 M) was used as an electrolyte.

Both acidic and basic titrations were performed starting from a pH of 5.5 for all the samples, with instrument washing with ultrapure water in between each step. Two different couples of samples per glass were used respectively for the acidic and basic titration. An adjustable gap cell was

used for the measurements. The gap between a couple of samples was adjusted to approximately 100 μm and the electrolyte flow to 100 mL/min, as suggested by the instrument provider [37].

2.3. In vitro antibacterial activity

2.3.1. Bacterial strains growth conditions

Bacteria were purchased from the American Type Culture Collection (ATCC, Manassas, Virginia, USA). To test SBA3 specimens' antibacterial and antibiofilm activity, the Gram-positive *Staphylococcus aureus* Multi-Drug resistance (*S. aureus* MDR, ATCC 43300) was used as representative of the pathogens affecting bone implants after surgery and in the case of severe infection, extra surgeries are required to remove the infected implants [38]. Bacteria were cultivated on Trypticase Soy Agar (TSA, Merck, Milan, Italy) and incubated at 37 °C until round single colonies were formed; afterward, some colonies were collected and diluted into 20 mL of Luria Bertani broth (LB, Merck, Milan, Italy). Broth cultures were incubated overnight at 37 °C under agitation (120 rpm in an orbital shaker). A fresh broth culture was prepared before each experiment to test bacteria in their exponential growth phase; accordingly, bacteria concentration was further diluted into fresh LB broth to a final concentration of 1×10^3 cells mL^{-1}, corresponding to an optical density (OD) of 0.00001 at wavelength 600 nm determined by spectrophotometer (Spark, Tecan, Switzerland). Fresh LB medium was used as a blank to normalize the OD values.

2.3.2. Antibacterial activity evaluation

Prior to biological assays, the samples were sterilized at high temperature (at 100 °C for 1 h). Two different protocols, the ISO 22196 standard and the one that has been published by the authors [33] considered here as UPO protocol were used to investigate antibacterial, antiadhesive, and antibiofilm properties of specimens towards *S. aureus* MDR. The international standard ISO 22196 protocol is designed to analyze the antibacterial behaviour of samples' surfaces by exposing them directly to a bacterial suspension [39]. Instead, the UPO protocol aims to investigate bacterial adhesion to the specimens' surfaces and then evaluate the antibiofilm properties of samples by forcing bacterial strains to create microcolonies or biofilm onto their surfaces.

To perform ISO22196 standard protocol, the sterile specimens were located into a 24-multiwell plate, and then, 50 μL of the bacterial suspension was directly dropped onto the specimens' surface and covered with a sterile polyethylene film. The inoculated specimens were placed in an incubator at 37 °C for 24 h. Afterward, the colorimetric metabolic assay (AlamarBlue™, Life Technologies, Milan, Italy) was applied to test viable bacteria metabolic activity by spectrophotometry following the manufacturer's instructions. Briefly, the ready-to-use Alamar blue solution at concentration 0.0015% was added to each well containing the test specimen (1 mL per specimen), and the plate was incubated in the dark for 4 h at 37 °C allowing resazurin dye reduction into fluorescent resorufin upon entering living cells. Then, 100 μL were spotted into a black-bottom 96-multiwell plate to minimize the background signal. The metabolic activity of bacteria was measured via fluorimetric analysis (λex = 570 nm and λem = 590 nm), and results were presented as Relative Fluorescent Units (RFU); Alamar blue solution (intended as cells-free) fluorescence was considered blank. Then, each specimen was washed with phosphate buffer solution (PBS, 1 mL) sonicated (5 min, 3 times), and vortexed (30 s, 3 times) to recover the bacteria. The colony-forming units (CFU) were counted by mixing 20 μL of bacteria with 180 μL of PBS and performing six-serial 10-fold dilutions as previously described by the Authors [33,40]; the total CFU count was done applying the following formula:

$$CFU = [(\text{number of colonies} \times \text{dilution factor})^{((\text{serial dilution}))}]$$

Then, scanning electron microscopy (SEM, JSM-IT500, JEOL, Tokyo, Japan) imaging was used to investigate the bacterial microcolonies or biofilm formed on the samples' surfaces; briefly, specimens were dehydrated by the alcohol scale (70–90–100% ethanol, 1 h each), swelled with hexamethyldisilazane, mounted onto stubs with conductive carbon tape and covered with a gold layer. Images were collected at different magnifications using secondary electrons detector.

In the UPO protocol, the sterile samples were transferred in a 24-multiwell plate and submerged fully into 500 μL of LB broth including 1×10^3 cells mL^{-1} of *S. aureus* MDR (as explained in detail in section 2.3.1). The multiwell plate was incubated at 37 °C and agitated on a small bench shaker (BenchRocker™ 3D, Sayreville, USA) at 100 rpm; afterward, the metabolic activity of adherent bacterial strains, viable CFU count, and SEM analysis were performed after two different time points: early time point (6 h) and late time point (24 h) to evaluate antiadhesive and antibiofilm properties of Cu doped SBA3 in comparison to undoped SBA3, respectively. To create a bacterial biofilm on specimens' surfaces, after 6 h of agitation at 100 rpm, the surplus of LB broth containing planktonic bacteria were removed from the wells and replaced with 1 mL of fresh LB broth to allow surface-adherent bacterial microcolonies to grow and form a layer of biofilm; after 24 h of incubation, antibiofilm properties of the Cu doped SBA3 were compared to undoped SBA3 as a control sample. After each time point (6 and 24 h), the specimens were washed with sterile PBS to remove non-adherent bacterial cells and bacterial metabolic activity and bacterial viable colonies were analyzed as mentioned above by colorimetric metabolic assay and CFU; the obtained results were visually confirmed by SEM.

Finally, the results of CFU count were expressed by means of antibacterial activity (R) indicating the effectiveness of an antibacterial agent, which was calculated according to the ISO 22196 protocols as follows [41]:

$$R = (U_t - U_0) - (A_t - U_0) = U_t\text{-}A_t$$

Where.

R is the antibacterial activity;
U_0 is the average logarithm of the number of viable bacterial colonies recovered from the untreated test specimens immediately after inoculation;
U_t is the average logarithm of the number of viable bacterial colonies recovered from the untreated test specimens after 24 h;
A_t is the average logarithm of the number of viable bacterial colonies recovered from the treated test specimens after 24 h.

2.4. Statistical analysis of data

Experiments were performed in triplicate. Results were statistically analyzed using the SPSS software (v.20.0, IBM, USA). First, data normal distribution and homogeneity of variance were confirmed by Shapiro-Wilk's and Levene's test, respectively; then, groups were compared by the one-way ANOVA using Tukey's test as post-hoc analysis. Significant differences were established at $p < 0.05$.

3. Results and discussion

The ion exchange in Cu(II)acetate solution was performed in three different concentrations 0.05 M, 0.01 M, and 0.001 M. Fig. 1 shows the surface morphology of SBA3 discs before and after ion exchange.

For all ion-exchanged samples (Fig. 1), some precipitation layers were observed on the surfaces compared to the undoped SBA3 surface. With a higher concentration of the ion exchange solution, a more evident surface layer was detected compared to the pristine SBA3 surface. The 0.001 M ion-exchanged surface was found to have only a few precipitates compared to higher concentrations. When further analyzing the elemental composition of the detected crystals by EDS analysis (Figs. 2 and 3), it was evident that they contained a large amount of Cu, also a higher amount of Cu was detected on the surface precipitation by using a greater concentration of Cu in the ion-exchange solution.

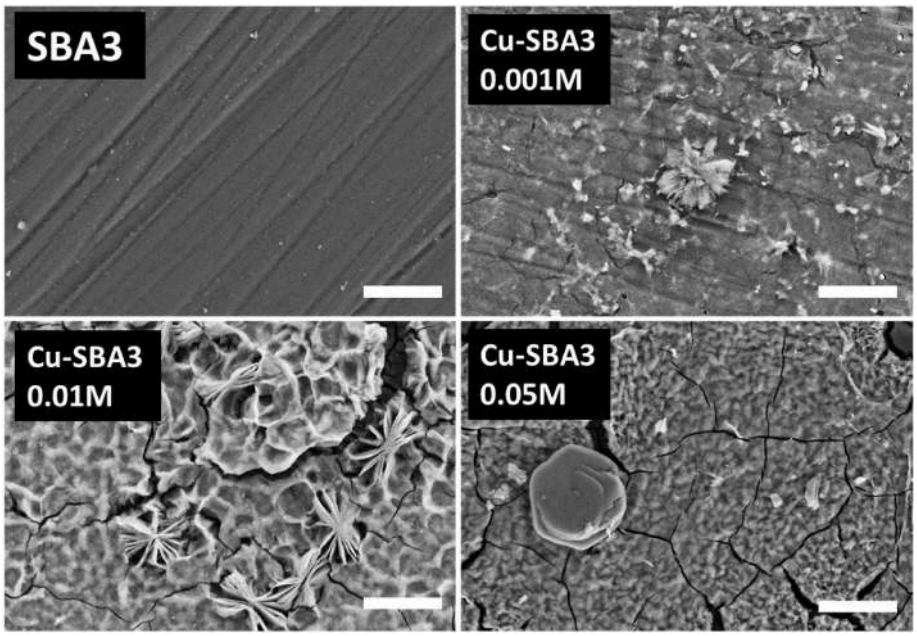

Fig. 1. FESEM images on the surface of SBA3 before and after ion exchange in Cu(II) acetate solution with different concentrations. Scale bars 10 μm.

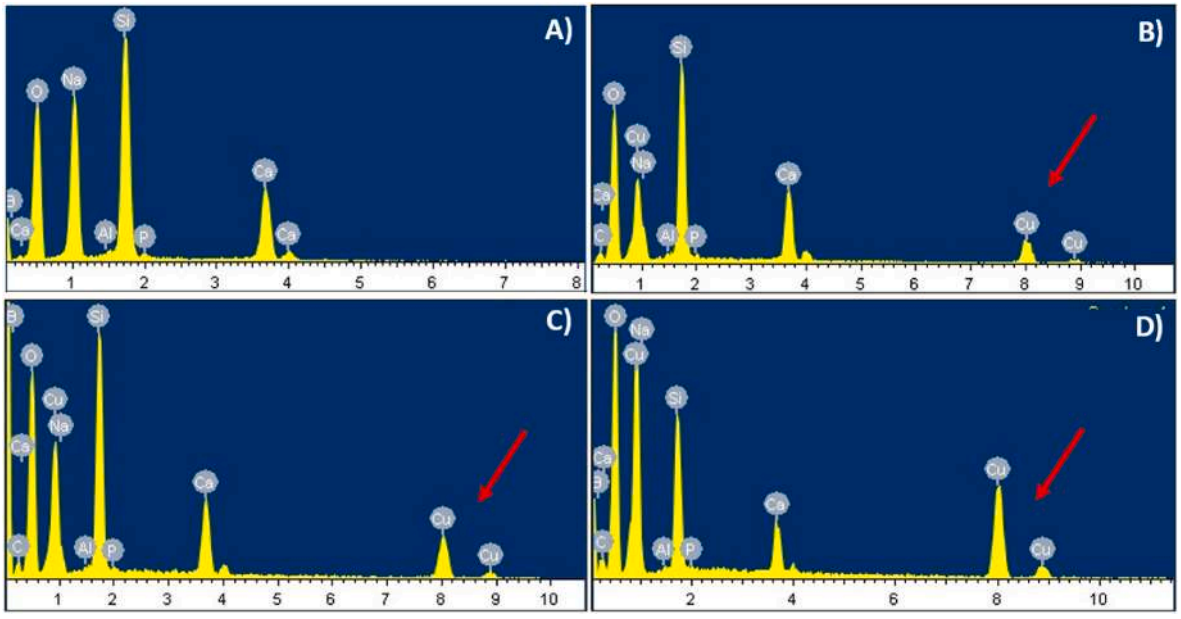

Fig. 2. EDS analysis of the surface of ion-exchanged samples, using A) Undoped SBA3, B)0.05 M solution (Cu-SBA3 0.05 M), C) 0.01 M solution (Cu-SBA3 0.01 M), and D) 0.001 M solution (Cu-SBA3 0.001 M) of Cu(II) acetate.

As can be observed in Fig. 3, the compositional EDS analysis from the surface of sample discs before and after ion exchange confirmed the presence of all the elements characteristic of the SBA3 and Cu-doped SBA3 glasses. However, boron is excluded from EDS analysis due to its low atomic weight and hence low detectability. When comparing glasses before and after ion exchange, Cu^{2+} seems to replace the sodium (Na^{+}) and calcium (Ca^{2+}) on the surface, which is seen as a reduction of those elements within ion-exchanged surfaces. It is also evident that the more concentrated ion exchange solution leads to greater replacement of Na^{+} and Ca^{2+} by Cu^{2+} on sample surfaces. For both the highest concentrations, the atomic percentage of Cu was found to be very high: for 0.05 M around 50 at-%, and 0.01 M 20 at-%. This information, combined with the high number of precipitates on the surfaces of 0.05 M and 0.01 M Cu-SBA3, the lowest concentration (0.001 M) seems the most suitable for biomedical applications and it is chosen to be further analyzed.

However, even though in the FESEM images (Fig. 1) some precipitations were present on the ion-exchanged surfaces, the XRD analyses of the surfaces (Fig. 4) did not detect any additional crystalline phases, except for the highest concentration tested. However, this result was expected as XRD analysis has a high penetration depth, and the phase detection has its limitations with phases present in very small amounts [42]. For Cu-SBA3 0.05 M, two peaks were detected approximately at 19°, and 28°, corresponding to copper acetate hydroxide hydrate $C_2H_6Cu_2O_5{\cdot}H_2O$ (ref 00-050-0407), which was expected considering the Cu(II)acetate solution used for the ion-exchange process. These results are in agreement with the previous analysis where no

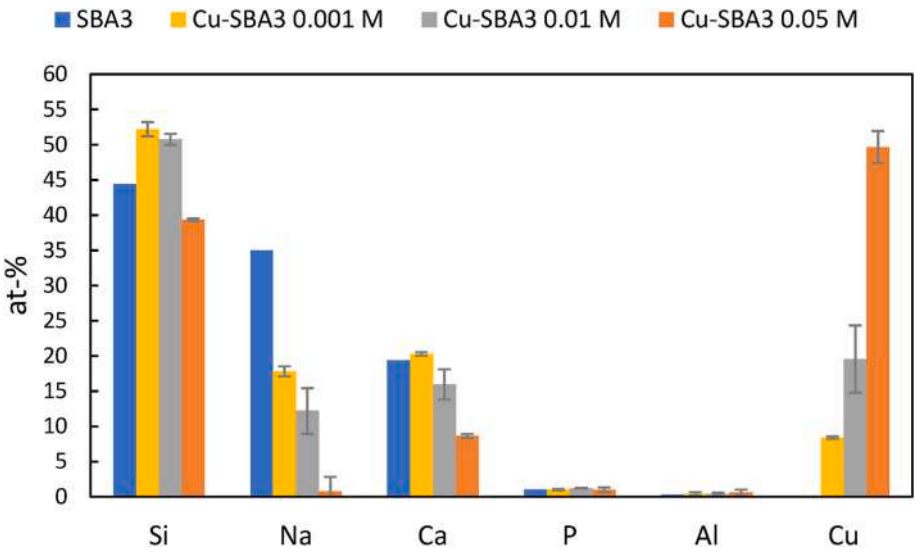

Fig. 3. EDS analysis of SBA3 and Cu-SBA3.

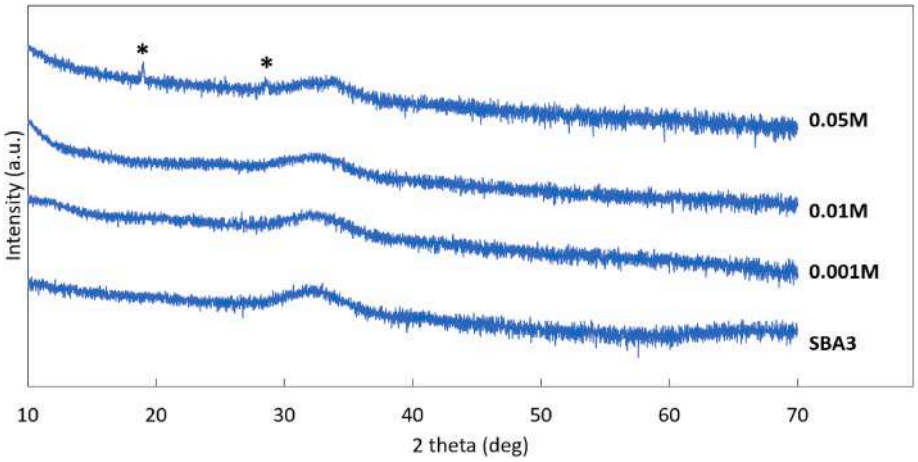

Fig. 4. Optimization of the ion-exchange process: XRD patterns of undoped SBA3 and Cu-SBA3 ion-exchanged in different concentrations. *) $C_2H_6Cu_2O_5{\cdot}H_2O$.

crystalline phases were detected when using similar ion-exchange process parameters [31].

Based on the morphological and phase analysis, the lowest ion-exchange concentration (0.001 M) was chosen to be further studied. The pristine SBA3 and the chosen ion-exchange concentration Cu-SBA3 0.001 M were also subjected to *in vitro* bioactivity test in SBF. The goal was to evaluate whether the introduction of Cu^{2+} through ion exchange would impact the hydroxyapatite formation, and hence, bioactivity.

The SEM/EDS analysis of SBF-soaked samples is shown in Fig. 5.

The samples soaked for 28 days are not shown because the results were very similar to the 14 days ones. The typical morphology of *in vitro* grown hydroxyapatite was detected for both undoped and doped discs after 7 days of soaking in SBF. Before that (1–3 days), silica gel formation occurred (cracks are due to the drying step before SEM observation). Regarding the EDS analysis, only a qualitative analysis of the Ca and phosphorus (P) peaks was possible instead of a quantitative one. This is due to the use of platinum (Pt) coating on the specimens, and the Pt peak is known to overlap with the P peak. However, the Ca and P content increases after 7 days for both undoped and doped specimens, also evidencing the presence of a Ca and P rich layer.

XRD analysis was carried out to confirm the presence of hydroxyapatite on glasses surface. Fig. 6 shows the XRD spectra from the two specimens before and after SBF immersion for up to 28 days.

For the SBA3 specimen before ion exchange, a broad halo between 2 theta 20° and 25°, which is attributed to silica gel formation, was noticed approximately after 3 days of soaking in SBF. Regarding the Cu-SBA3 0.001 M, a peak corresponding to hydroxyapatite was already detected after the 3-day soaking. Moreover, hydroxyapatite precipitation seems more evident also on the later time points for Cu-SBA3, suggesting that the Cu^{2+} addition by ion exchange could enhance the hydroxyapatite formation. However, as demonstrated in the EDS compositional analysis (Fig. 3), Cu was found to partially substitute Na and Ca on the glass, which could be hypothesized to lead to decelerated dissolution rate of the glass. Still, it should be noted that the Cu is introduced only to the very surface of the glass as a thin layer, where it unlikely has a great impact on the glass bulk properties. In the literature, there is no consensus on the effect of Cu inclusion on the BAG hydroxyapatite-forming ability, and hence, bioactivity [5]. In some studies, the bioactivity mechanism was found to be improved by adding a Cu precursor to bioactive glass nanoparticles [43], while, according to other studies, Cu addition as an oxide to melt-derived borosilicate glass foam scaffolds lead to a more stable glass network and lower degradation ability [44]. However, in both mentioned experiments Cu was introduced using different approaches and the used BAG was not used as a bulk, which makes comparison difficult.

Considering the Cu^{2+}-ion release from the BAG surface, a leaching

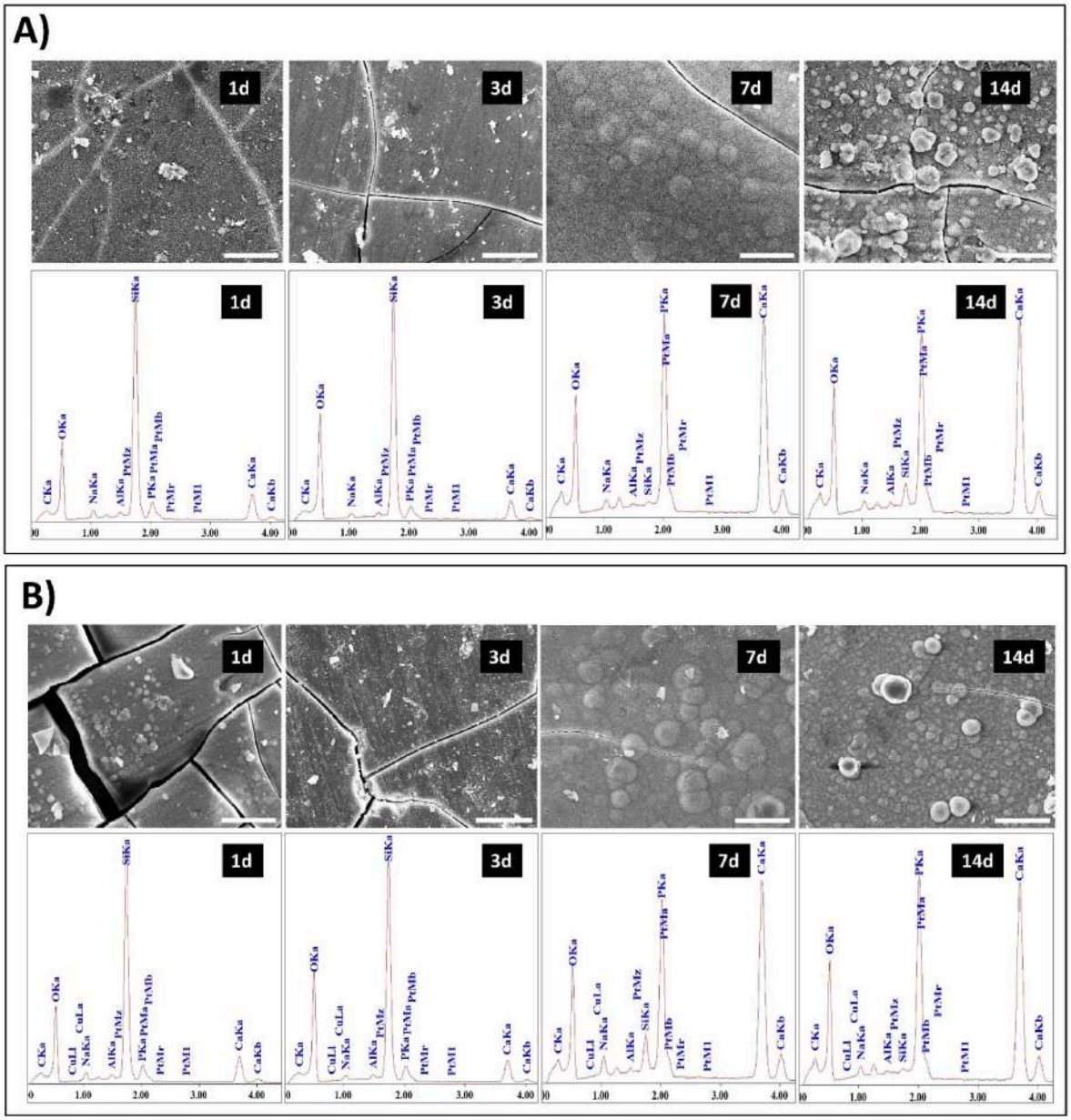

Fig. 5. SEM/EDS analysis of SBF-soaked A) control specimens (SBA3), and B) Cu-doped specimens (Cu-SBA3 0.001 M). Scale bars 20 μm.

test was performed both in physiological (SBF, pH 7.4) and inflammatory pH (HAc/NaAc buffer, pH 5.0). The experiment was performed only for the lowest ion exchange concentration of 0.001 M (Cu-SBA3 0.001 M). The pH evolution and the release of Cu^{2+} in both soaking solutions are demonstrated in Fig. 7.

Regarding the pH value of SBF during the soaking of Cu-SBA3 (Fig. 7A), there were no significant differences observed. It is noteworthy that pH5 acetate buffer exhibited a lower buffering capacity and displayed a consistent increase in pH over the 28-day soaking period (Fig. 7B). The pH increased from a slightly acidic level to a neutral pH of around 7. These phenomena can likely be attributed to the different acid-base characteristics of the two buffer solutions. The sodium acetate buffer is based on a weak acid (acetic acid) with a buffering range of approximately 3.6–5.6 and a pKa value of 4.76 [45]). On the other hand, the SBF is buffered with TRIS-buffer, based on a stronger acid (HCl) with a buffering range of pH 7.0 to 9.0. During the soaking process, bioactive glasses tend to rapidly release ions into the aqueous environment, leading to an increase in pH towards more alkaline values. Consequently, the buffering capacity of the acetate buffer in our particular case was comparatively more limited due to its weaker acid-base characteristics.

As seen in Fig. 7, the major amount of Cu^{2+} seems to be released from the glass during the first three days of soaking, independent of the soaking solution. A similar trend was found in the previous work where Miola et al. found the majority of Cu^{2+} release from Cu-doped glass/PMMA composites during the first days of the soaking, but on the contrary, they did not detect a plateau similar to what was found in present work after around 3 days of soaking in both conditions [26]. It must be underlined that in the mentioned study the Cu-doped glass was uniformly dispersed into a PMMA matrix [26], while in the present paper, low amounts of Cu^{2+} ions are concentrated on the glass surface and can be fast released. The decrease of the Cu concentration in solution at 7 days can be related to the precipitation of hydroxyapatite, which occurs mainly from day 7, as detected by SEM observations (Figs. 5 and 6), and could involve the re-precipitation of Cu^{2+} ions that can partially replace Ca^{2+} ions in the hydroxyapatite lattice, as reported in the literature [46,47]. This

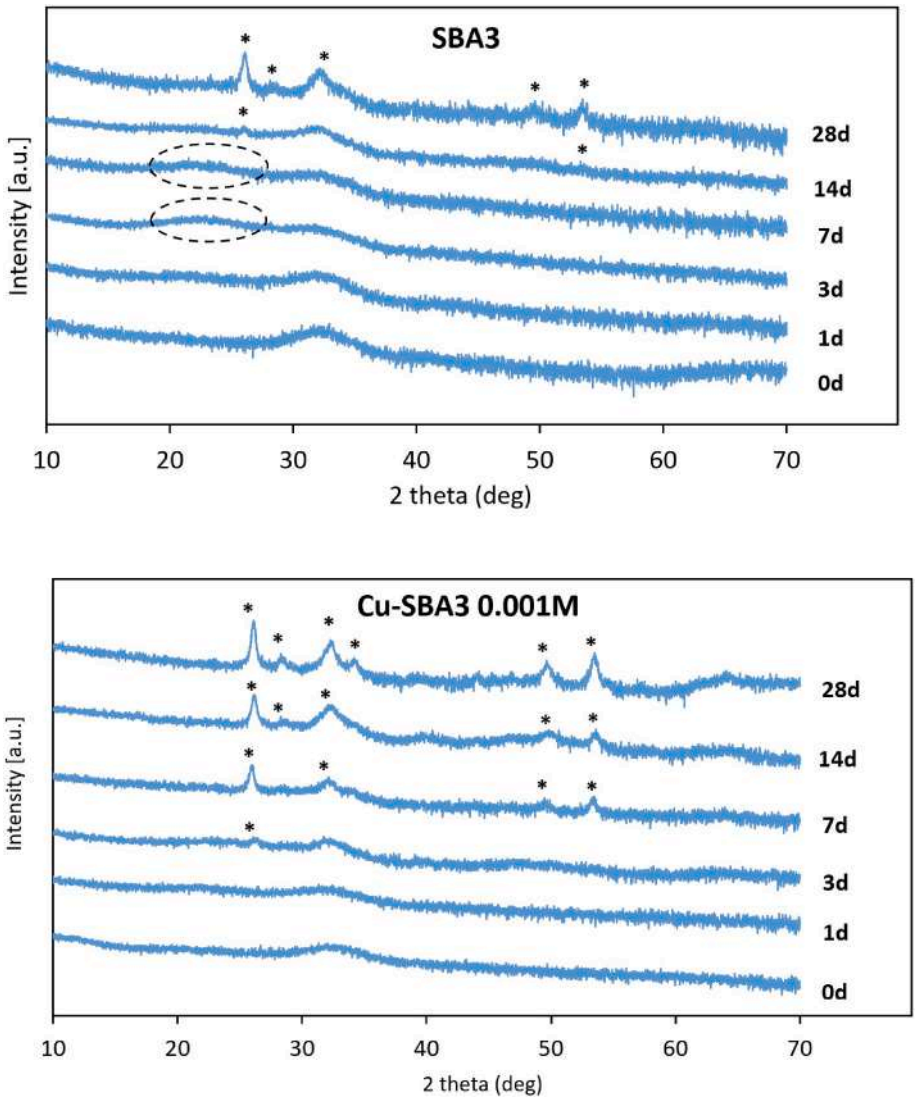

Fig. 6. XRD patterns of pristine and SBF-soaked SBA3 and Cu-SBA3 0.001 M. (– -) silica gel, *) hydroxyapatite.

hypothesis could be strengthened by further phase analysis, for example by estimating the average crystallite size and lattice parameters, but this is out of the aim of the present paper. A further release can be observed from day 7 on, which can be explained by the Cu^{2+} confinement on the very outer glass surface, that reasonably does not negatively affect the ion release involved in the bioactivity mechanism, as already observed by authors in a previous paper [31]. When comparing the Cu^{2+}-release in SBF and inflammatory condition-mimicking buffer solution, no notable differences were detected. The HAc/NaAc buffer-soaked specimens initially showed a slightly higher release of Cu^{2+} ions than the SBF solution. This phenomenon is also reported in other studies, for example, Bingel et al. reported that in general lower pH of the used immersion, the solution increases ion release due to more protons being available for ion exchange reactions between glass modifier ions and protons from the dissolution medium [36,48]. However, the effect of solution pH on Cu^{2+} ion release specifically has not been previously reported. The ICP analysis including all the ions releasing from the glass instead of only Cu^{2+} could bring more clarity to this hypothesis. In addition, the more aggressive initial ion release during the first 3 days of soaking could also explain the more prevalent Cu^{2+} re-precipitation after 14 soaking in HAc/NaAc compared to SBF.

Zeta potential titration measurements were performed both on pristine SBA3 and ion-exchanged Cu-SBA3 (Figs. 8 and 9) before (0 day) and after different times of soaking in SBF (1-7-28 days).

The isoelectric point (IEP) of both unsoaked SBA3 (SBA3 0d) and ion-exchanged unsoaked Cu-SBA3 (Cu-SBA3 0d) was around 3.4, which indicated that both surfaces had a small prevalence of acidic functional groups (supposedly OH groups) since an IEP of 4 is expected for a surface without the prevalence of any charged functional groups [37]. Both curves had a plateau with onset at pH 5.5, due to acidic functional groups completely deprotonated at any pH higher than 5.5 on both glasses [49].

A different slope of the curves was noticed on SBA3 and Cu-SBA3 at a pH around the IEPs. SBA3 was more hydrophobic, the water molecules were weakly adsorbed, and they were easily replaced by the hydroxyl (in the basic range) or hydronium ions (in the acidic range) in the solution. The observed larger hydrophilicity on Cu-SBA3 can be related to a larger amount of total hydroxyl groups on the surface. An evident increase in the standard deviation of zeta potential, around the IEP and below it, evidenced a strong reactivity of both surfaces in a very acidic environment [50].

Looking at the gap variation during the pH titration, a reduction of the gap (few micrometers) was observed on SBA3 both in the acidic and in the basic range attributable to the formation of a silica gel layer and a small expansion of the sample; the lowest significant variation of the gap is about 5 μm. Almost no gap variation was registered on Cu-SBA3

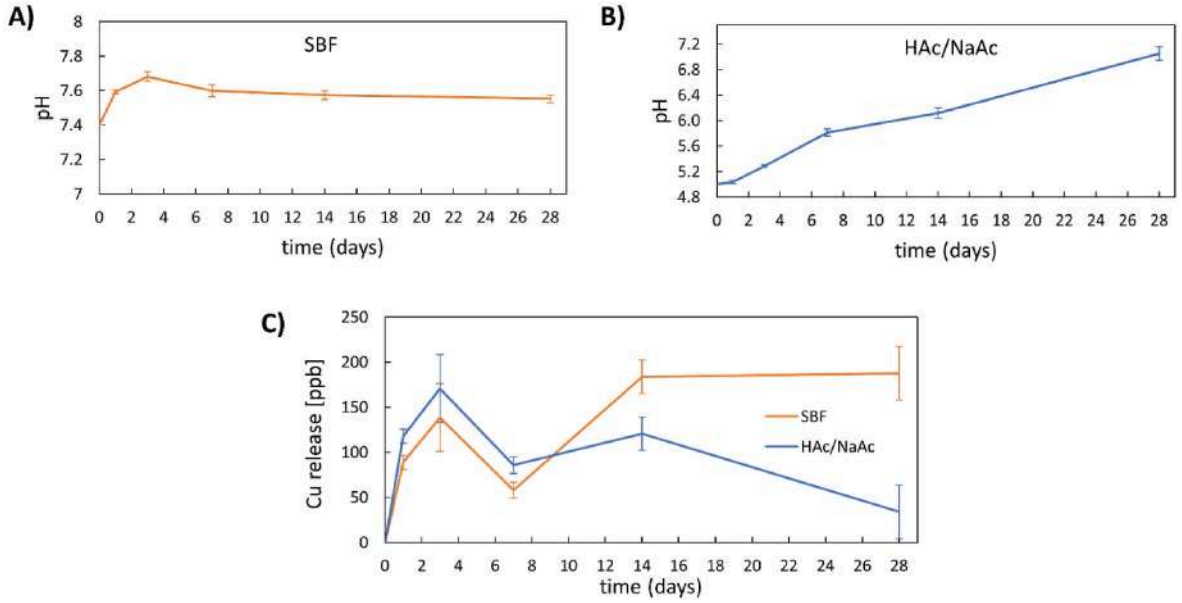

Fig. 7. A) pH evolution of SBF solution as a function of time of Cu-SBA3 soaking, B) pH evolution of pH5 acetate buffer as a function of time of Cu-SBA3 soaking, and C) Release of Cu^{2+}-ions from glass surface as a function of soaking time in SBF (orange)or pH5 acetate buffer (HAc/NaAc, blue). (For interpretation of the references to color in this figure legend, the reader is referred to the Web version of this article.)

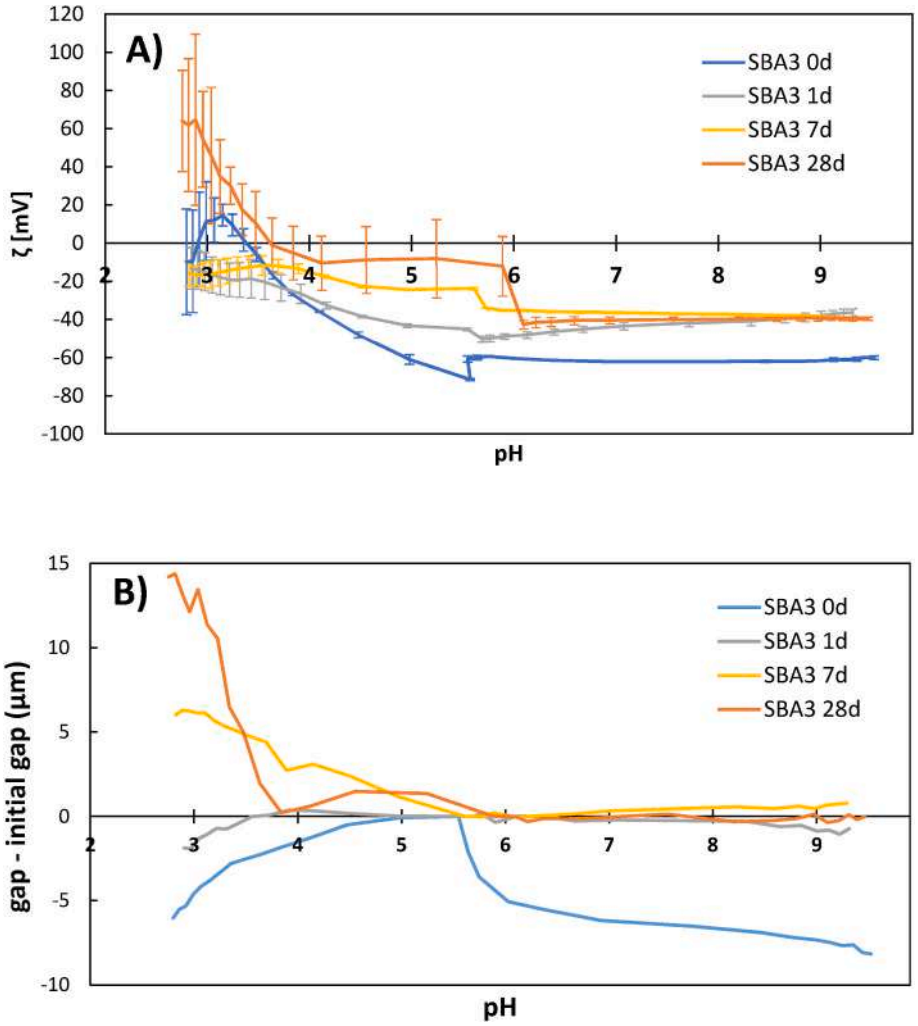

Fig. 8. Zeta potential titration curves (A) and gap variation (B, measured gap – initial gap) of SBA3 before and after soaking in SBF.

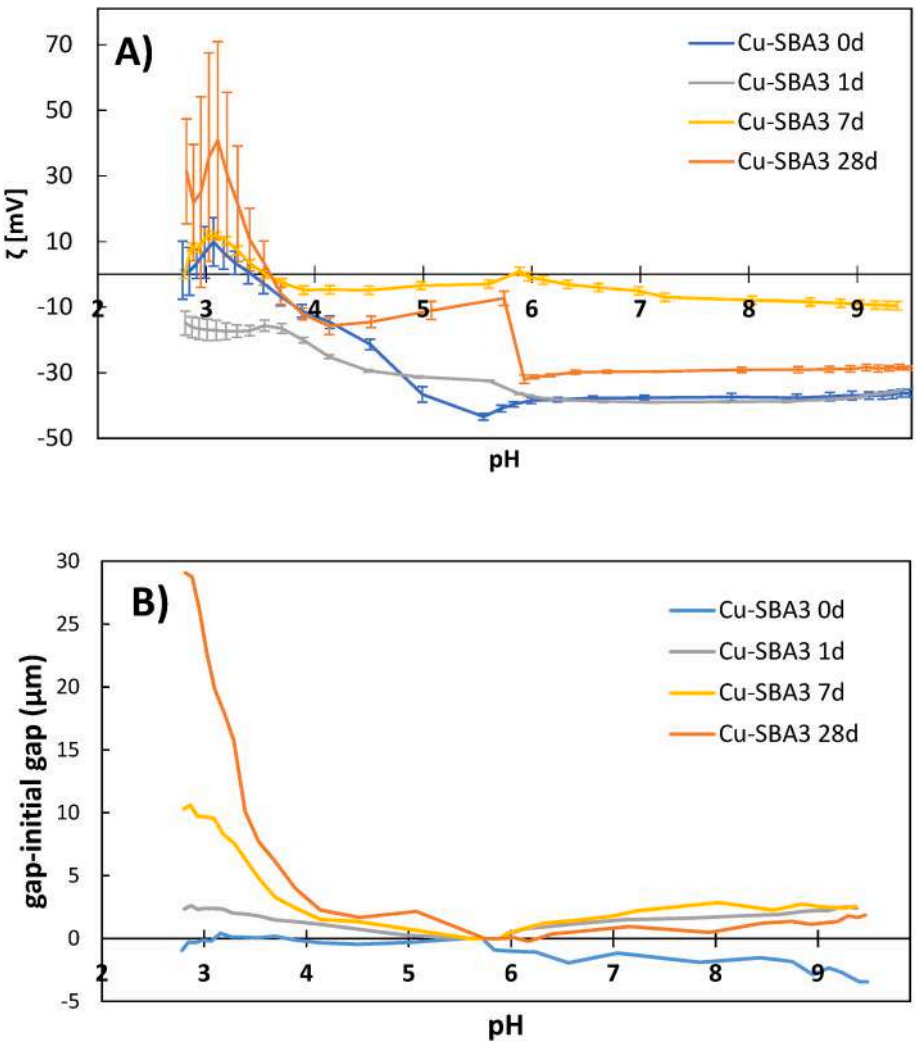

Fig. 9. Zeta potential titration curves (A) and gap variation (B, measured gap – initial gap) of Cu-SBA3 0.001 M before and after soaking in SBF.

during the pH titrations evidencing a different type of silica gel layer.

As a reference of the soaked samples, the IEP of synthetic hydroxyapatite is reported to be around 5.5, it has a zeta potential of about −30 mV at any pH higher than 6 [51], and dissolution of hydroxyapatite formed on bioactive materials is reported at a pH lower than 4 [50]. None of the soaked samples had an IEP close to the value of synthetic hydroxyapatite. The measured IEPs were close to those of the glasses before soaking or not detectable (as in the case of SBA3 and Cu-SBA3 soaked for 1 day and SBA3 soaked for 7 days). The standard deviations of the curves of the soaked samples had an evident increase at a pH lower than 4. The deviation of the gap was negative, and it was evident below pH 4 on the samples soaked for 7–28 days. All the curves had a plateau in the basic pH range, with an onset around pH 6, and a value of about −30 mV. All obtained data can be interpreted considering that the formed hydroxyapatite was dissolved and detached from the substrates when pH went down below pH 4, the detachment exposed the glass surface, and the IEP of hydroxyapatite was not measured. On the other side, hydroxyapatite was almost stable in the basic range (no gap variation detected, low standard deviation of zeta potential, and a plateau at a zeta potential value close to that of hydroxyapatite). The thickness of the detached surface layer was higher in the case of Cu-SBA3 than on SBA3. This result agreed with the larger amount of hydroxyapatite registered through XRD on Cu-SBA3 after soaking. The samples soaked for 1 day did not have a detectable detachment of hydroxyapatite because of its low thickness, in agreement with XRD, but their curves were clearly different from those of the as-prepared glasses evidencing their surface reaction in SBF.

These data can be compared with a similar work performed on SBA2, a glass with a lower Na_2O amount (18 mol% vs. 26 mol%) [49,50]. The main difference between the glasses was the reactivity of SBA2 in the basic range (pH > 8) while SBA3 was in the acid. Cu-SBA3 soaked for 28 days showed a larger detachment and thicker layer of hydroxyapatite than both SBA2 and SBA3. The curve of SBA3 soaked for 7 days was similar to SBA2 soaked for 7 days: a low zeta potential value along the whole titration curve. It can be explained by the evolution of hydroxyapatite during its maturation [50]. The shape of the curve of SBA3 soaked for 7 days was not far from SBA3 soaked for 1 day, according to the low bioactivity of this glass.

According to the results obtained from the morphological and glass surface phase analyses (detailed in previous sections) of Cu^{2+}-doped samples in ion-exchanged solution with different concentrations of Cu^{2+} (0.001, 0.01, and 0.05 M), SBA3 in the lowest concentration of the ion-exchanged solution (Cu-SBA3 0.001 M) was chosen for *in vitro* biological assessments. To differentiate between the antibacterial and antibiofilm properties of specimens towards *S. aureus* MDR, two different protocols were used: ISO 22196 standard protocol for antibacterial evaluation and UPO protocol for antiadhesive and antibiofilm evaluation (detailed in section 2.3.2) [39]. Fig. 10 (A-C) shows the results of metabolic activity, bacterial colonies count (CFU), and SEM that were obtained from ISO22196 standard protocol. After 24 h of direct inoculation of *S. aureus*

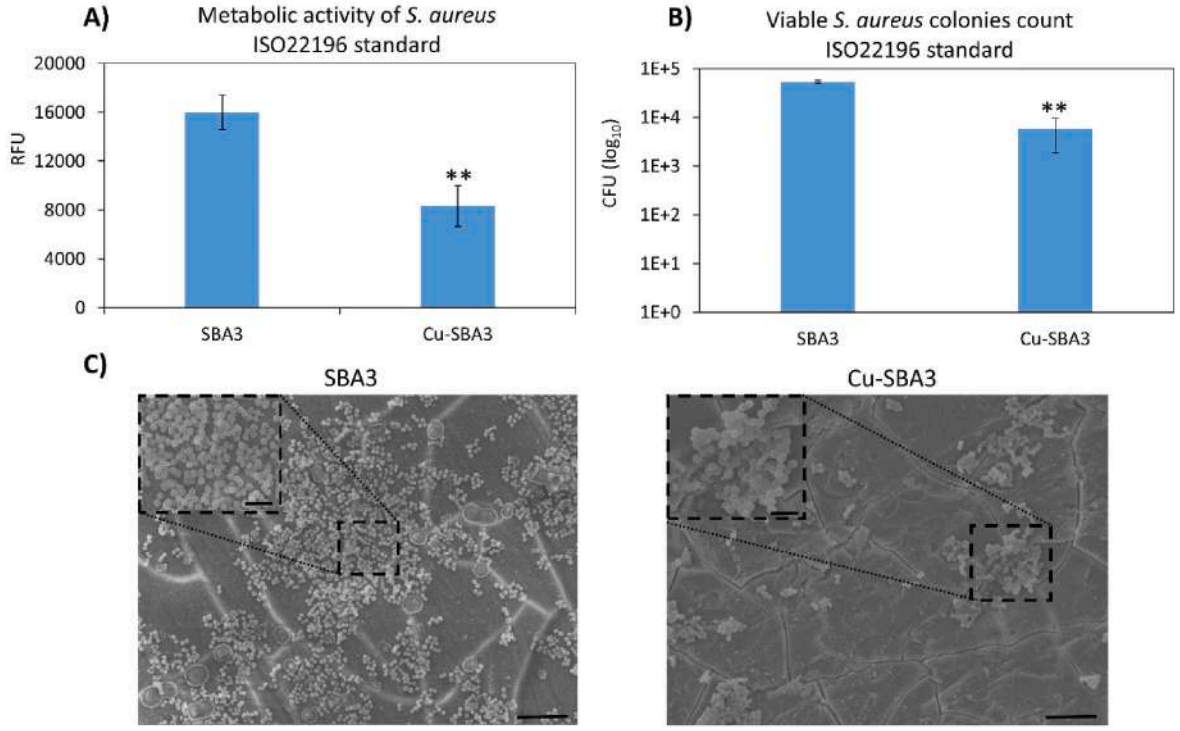

Fig. 10. Antibacterial test according to ISO 22196 standard after 24 h incubation at 37 °C: A) Metabolic activity of *S. aureus* MDR on the specimens' surfaces; B) Viable surface-attached bacterial colonies count (CFU), C) SEM images taken in two different magnifications (1500X in the image and 4000X in the left corner inset with scale bars 10 and 5 μm respectively). ** indicates p value < 0.01 and bars represent standard deviations.

on the samples' surfaces, metabolic activity analysis of bacterial strains showed a statistically significant difference of ~52% between Cu doped SBA3 and undoped SBA3 (Fig. 10 A; $p < 0.01$ represented by **). Additionally, surface-adherent viable bacterial colonies count (CFU) revealed that the number of bacterial cells attached to Cu-SBA3 surfaces was approximately 1 log less than the ones attached to the control samples (Fig. 10 B; $p < 0.01$ indicated by **). This difference in metabolic activity and the number of surface-attached bacterial cells between CU-SBA3 and undoped SBA3 was visually confirmed by means of SEM images that were taken in two different magnifications (1500X and 4000X, Fig. 10 C). As shown in the SEM image of undoped SBA3, most part of the control sample surfaces was covered by a layer of bacterial biofilm; while few aggregations of bacterial cells were observed on the surface of Cu-SBA3, in agreement with ~52% and ~1 log reduction of metabolic activity and viable bacterial colonies count, respectively.

To evaluate the specific behavior of the doped samples (Cu-SBA3) concerning bacterial adhesion and biofilm formation, the UPO protocol was utilized. In this case, the sterile samples were fully submerged into 500 μL of *S. aureus* MDR suspension and the impact of Cu-SBA3 on bacterial attachment and biofilm formation was evaluated by measuring bacterial metabolic activity, surface-adherent CFU and SEM at two different time points: i) early time point (6 h) that it was selected based on the results obtained from ion release evaluation (Fig. 7); as shown in Fig. 7, Cu^{2+} released from the samples' surfaces during the first 3 days of soaking in the SBF and inflammatory solution (acetate buffer at pH 5). Therefore, 6 h was chosen to evaluate whether Cu-doped SBA3 was able to decline bacterial adhesion on the samples' surfaces or not; ii) late time point (24 h) to investigate the effect of Cu-SBA3 on bacterial biofilm formation onto the samples' surfaces. The results of bacterial metabolic activity, adherent viable colonies count, and SEM are presented in Fig. 11 A-C. According to the results of metabolic activity and CFU, after 6 h of bacterial inoculation onto the specimens' surfaces and incubation, no statistically significant difference in adherent bacteria was observed between Cu-SBA3 and undoped SBA3 (control sample) surfaces. However, after 24 h, the metabolic activity of *S. aureus* MDR showed a reduction of approximately 52% on the Cu-SBA3 surfaces in comparison to undoped SBA3 (p-value <0.01 indicated by **; Fig. 11 A); in addition, CFU count results demonstrated that adherent bacterial colonies onto the Cu doped samples' surfaces decreased about 0.6 log in comparison to attached colonies onto the control samples (p-value <0.05 indicated by *; Fig. 11 B). These results were in line with SEM images that were taken at two different magnifications (1500X and 4000X with scale bars 10 μm and 5 μm, respectively; Fig. 11 C). After 6 h, few bacterial colonies adhered to the samples' surfaces and no difference in colony number was observed between Cu-doped SBA3 and undoped SBA3 samples. After 24 h of inoculation and incubation, attached bacterial cells on the SBA3 samples' surfaces grew and bacterial microcolonies (biofilm) formed on the surfaces of control samples. While some single colonies detected on Cu-SBA3 surfaces indicating that released Cu^{2+} ions from the doped samples during 24 h in contact with bacterial suspension showed antibiofilm properties (Fig. 11 C) as the same results that were obtained from ISO protocol.

For both protocols (ISO 22196 standard and UPO protocol), antibacterial activity (R score) was calculated by the difference between the average of the common logarithm of the number of viable bacteria recovered from the undoped control samples (U_t) and doped ones (A_t) after 24 h; indeed, R score reveals the effectiveness of an antibacterial agent [39,41]. The results are presented in Table 1 as well as the count of the initial inoculum ($U_0 = 3.7$) that was confirmed in the magnitude of 5E3.

The results obtained from *in vitro* evaluation of antibacterial and antibiofilm properties for Cu^{2+} doped SBA3 in comparison to undoped SBA3 revealed that doped specimens in lower ion-exchange solution (0.001 M) had no impact on the attachment of *S. aureus* MDR on to samples' surfaces (after 6 h); while during 24 h, antibacterial and antibiofilm properties of Cu-SBA3 has initiated due to release of Cu^{2+} ions into the LB broth and both used protocols (ISO 22196 standard and UPO protocol) showed more or less the same results, a 50% reduction for

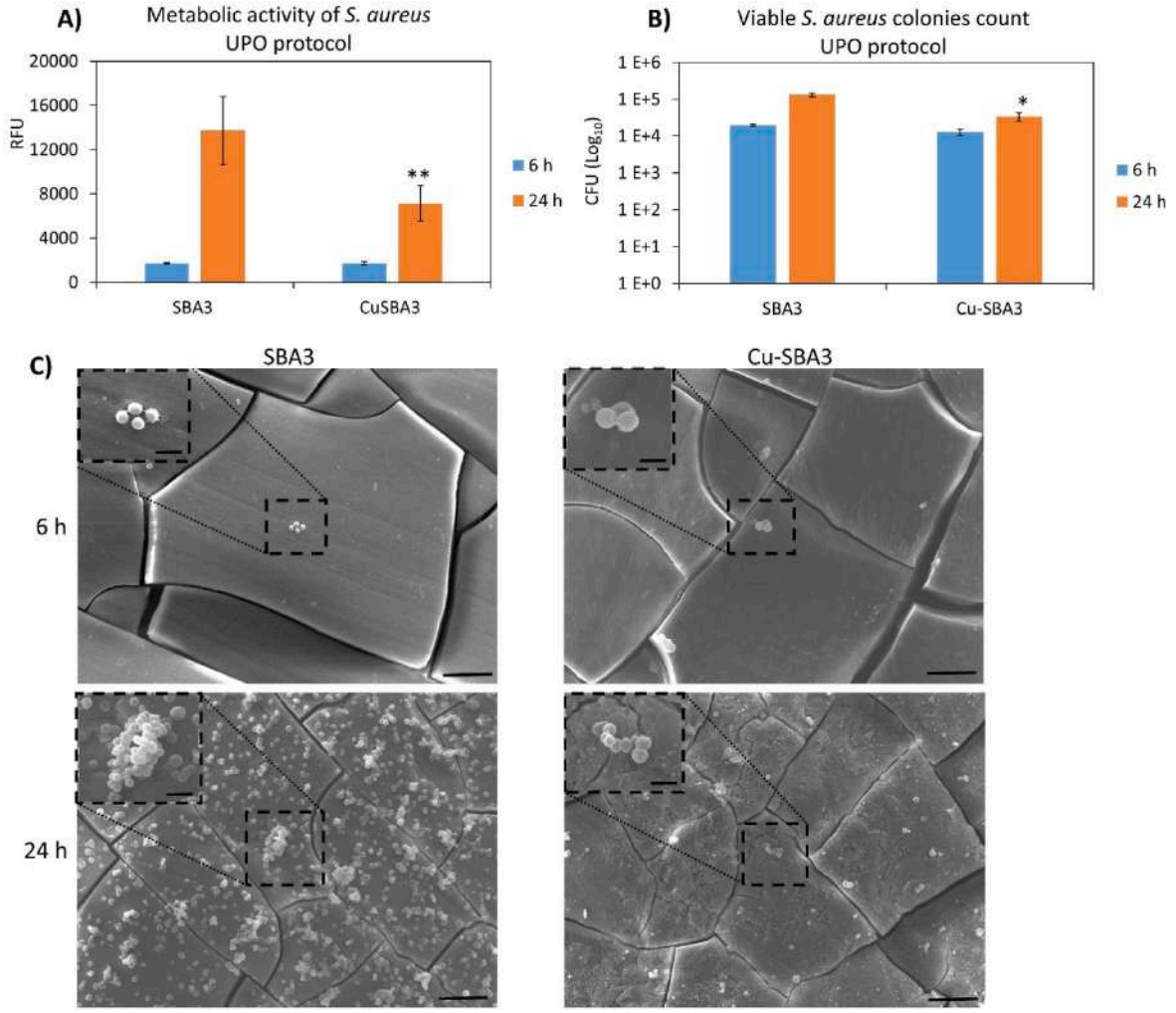

Fig. 11. Antiadhesive and antibiofilm test according to the UPO protocol after 6 and 24 h incubation at 37 °C, respectively: A) Metabolic activity of *S. aureus* MDR on the specimens' surfaces; B) Viable surface-attached bacterial colonies count (CFU), C) SEM images taken in two different magnifications (1500X in the image and 4000X in the left corner inset with scale bars 10 and 5 μm respectively). * and** indicate $p < 0.05$ and $p < 0.01$, respectively; bars represent standard deviations.

Table 1
R score values calculated by the colony-forming unit (CFU) count immediately after inoculation (U_0) and after 24 h of culture in direct contact with the specimens' surface (U_t for untreated and A_t for treated samples).

Sample	Protocol	Log_{10} CFU Count (U_0)	Log_{10} CFU Count (U_t, A_t)	(R) score
SBA3	ISO 22196	3.7	4.7	Control sample
Cu-SBA3	ISO 22196	3.7	3.7	1
SBA3	UPO	3.7	5.1	Control sample
Cu-SBA3	UPO	3.7	4.5	0.6

metabolic activity and between 0.6 and 1 log decrease for surface-adherent bacterial colonies. Moreover, from the result of the R score obtained from two investigated protocols (0.6 and 1 for UPO and ISO 22196 protocols, respectively), it was concluded that the effectiveness of Cu-SBA3 samples by using these two protocols was more or less the same.

These results are in agreement with previous literature. Pierre et al. investigated the biological properties of homogeneous calcium phosphate coating on titanium dental implants that were doped with Cu exchange post-treatment at different concentrations (0.001, 0.05, and 0.01 M) towards Gram-positive and Gram-negative bacterial strains at two time points (4 and 24 h). They reported that after 4 h, there was a low reduction of adherent Gram-negative onto the samples doped with Cu in comparison to undoped specimens, while for Gram-positive bacterial strains, no noticeable difference was observed. However, after 24 h of inoculation, a significant reduction of CFU of about 2 log for both Gram-positive and Gram-negative bacterial strains was observed [52]. Regarding Cu-doped bioactive glasses, Popescu et al. conducted a study on the antibacterial activity of Cu-containing bioactive glass-ceramics against *S. aureus*. They found that the glass with 0.5 mol% CuO exhibited the lowest minimum inhibitory concentration and bactericidal concentration against *S. aureus*. Additionally, they observed that the release of Cu^{2+} ions from this glass after 24-h soaking in deionized water was similar to the values measured in our study (Fig. 7C) [53]. In another investigation, which examined the effect of Cu^{2+}-ion release from a calcium-phosphate glass with varying Cu content on *S. aureus*, a strong correlation was found between the concentration of released Cu^{2+} and the bactericidal properties [54]. Nevertheless, while it is generally observed that higher copper content correlates with improved antibacterial performance, it is crucial to consider that elevated concentrations of copper can potentially generate an excessive quantity of free radicals, which may induce cytotoxicity [55]. Therefore, it is crucial to carefully control the release kinetics of copper to ensure an optimal

balance between antibacterial efficacy and potential cytotoxic effects.

Even though the here studied glass shows potential to be used as an antibacterial material it is pivotal to further assess its cytocompatibility and Cu^{2+} leaching in the used culturing conditions. Cu-SBA3 discs have been found to decrease human adipose stem cell viability in direct culture, possibly due to the rapid release of Cu^{2+} from glass surface in the cell culture [56]. Instead, when employing an indirect culture the cells stayed viable with healthy morphology, suggesting only contact killing phenomenon. However, these preliminary tests made with one cell line were only a starting point for deeper understanding of the cytocompatibility and possible osteogenic potential or angiogenic properties of the Cu-SBA3 glass.

4. Conclusion

In the present study, SBA3 bioactive glass surface was doped with ionic Cu^{2+} by an ion exchange process in an aqueous solution. First, the effect of the concentration of the used Cu(II)-rich ion exchange solution was studied by assessing the glass morphology, elemental composition, and amorphous nature. Based on these analyses the lowest concentration of 0.001 M of the ion exchange solution was chosen for further analyses. Next, the impact of the Cu-doping of the SBA3 surface on the amorphous nature, bioactivity, and chemical stability of the glass in both physiological and inflammatory pH ranges was investigated. The undoped SBA3 was used as a reference to Cu-doped SBA3. The Cu-doped SBA3 surface remained without any large precipitates of copper salts, hence confirming the amorphous nature of the glass. Interestingly, Cu-doping was also found not to negatively affect the bioactivity mechanism; instead, more enhanced formation of hydroxyapatite was seen on the Cu-SBA3 surface compared to the undoped SBA3 surface as evidenced by SEM-EDS, XRD, and zeta potential measurements. In addition, the antibacterial effect of the Cu-doping towards Gram-positive *Staphylococcus aureus* MDR was studied in detail by assessing anti-adhesive, antibacterial, and antibiofilm properties utilizing two different protocols (ISO 22196 standard and UPO protocol). The released Cu^{2+}-ions from doped samples showed no impact on bacterial adhesion onto the samples' surfaces determined by UPO protocol after 6 h. However, both protocols after 24 h revealed a noticeably significant reduction of bacterial metabolic activity (about 52%) and surface-adherent bacterial cells count (CFU, 0.6–1 log) using metabolic Alamar blue assay and CFU count. Results were visually confirmed by SEM images where few viable single colonies were observed on the Cu-SBA3 surfaces after 24 h of incubation with direct contact with *S. aureus* suspension. The here-described antibacterial ion-releasing bioactive glass represents a promising starting point for the realization of a non-antibiotic antibacterial materials for bone tissue engineering applications.

Author contributions

Conceptualization, E.V. and M.M.; methodology, E.V., M.M., S.S. and A.C.; investigation, M.L., M.M. and Z.N.; resources, L.R. and E.V.; writing—original draft preparation, M.L., Z.N., S.S., M.M. and E.V.; writing—review and editing, M.L., M.M., Z.N., A.C., S.S, L.R. and E.V.; visualization, M.L. and Z.N.; supervision, E.V.; project administration, L. R. and E.V.; funding acquisition, L.R. and E.V. All authors have read and agreed to the published version of the manuscript.

Declaration of competing interest

The authors declare that they have no known competing financial interests or personal relationships that could have appeared to influence the work reported in this paper.

Acknowledgements

This study was funded by the European Union's Horizon 2020 Research and Innovation Program under Marie Skłodowska-Curie grant agreement No 860462-Project PREMUROSA to L. Rimondini.

References

[1] W. Cao, L.L. Hench, Bioactive materials, Ceram. Int. 22 (6) (1996 Jan 1) 493–507.
[2] J. Rivadeneira, A. Gorustovich, Bioactive glasses as delivery systems for antimicrobial agents, J. Appl. Microbiol. 122 (6) (2017) 1424–1437.
[3] L. Drago, M. Toscano, M. Bottagisio, Recent evidence on bioactive glass antimicrobial and antibiofilm activity: a mini-review, Materials 11 (2) (2018 Feb 24) 326.
[4] A. Hoppe, V. Mouriño, A.R. Boccaccini, Therapeutic inorganic ions in bioactive glasses to enhance bone formation and beyond, Biomater. Sci. 1 (3) (2013 Mar 4) 254–256.
[5] S. Kargozar, M. Mozafari, S. Ghodrat, E. Fiume, F. Baino, Copper-containing bioactive glasses and glass-ceramics: from tissue regeneration to cancer therapeutic strategies, Mater. Sci. Eng. C 121 (2021 helmikuu), 111741.
[6] H.T. Michels, D.G. Anderson, Antimicrobial regulatory efficacy testing of solid copper alloy surfaces in the USA, Met Ions Biol Med 10 (2008) 185–190.
[7] A.G. Dalecki, C.L. Crawford, F. Wolschendorf, Chapter six - copper and antibiotics: discovery, modes of action, and opportunities for medicinal applications, in: R. K. Poole (Ed.), Advances in Microbial Physiology [Internet], vol. 70, Academic Press, 2017 [cited 2022 Sep 19]. pp. 193–260. (Microbiology of Metal Ions, https://www.sciencedirect.com/science/article/pii/S0065291117300073.
[8] M. Vincent, R.E. Duval, P. Hartemann, M. Engels-Deutsch, Contact killing and antimicrobial properties of copper, J. Appl. Microbiol. 124 (5) (2018) 1032–1046.
[9] C.E. Santo, D. Quaranta, G. Grass, Antimicrobial metallic copper surfaces kill Staphylococcus haemolyticus via membrane damage, MicrobiologyOpen 1 (1) (2012) 46–52.
[10] B.R. McAuslan, W. Reilly, Endothelial cell phagokinesis in response to specific metal ions, Exp. Cell Res. 130 (1) (1980 Nov 1) 147–157.
[11] G.F. Hu, Copper stimulates proliferation of human endothelial cells under culture, J. Cell. Biochem. 69 (3) (1998) 326–335.
[12] S. Li, H. Xie, S. Li, Y.J. Kang, Copper stimulates growth of human umbilical vein endothelial cells in a vascular endothelial growth factor-independent pathway, Exp. Biol. Med. 237 (1) (2012 Jan 1) 77–82.
[13] W. Feng, F. Ye, W. Xue, Z. Zhou, Y.J. Kang, Copper regulation of hypoxia-inducible factor-1 activity, Mol. Pharmacol. 75 (1) (2009) 174–182.
[14] Q. Li, feng, X. Ding, qin, Y.J. Kang, Copper promotion of angiogenesis in isolated rat aortic ring: role of vascular endothelial growth factor, J. Nutr. Biochem. 25 (1) (2014 Jan 1) 44–49.
[15] Xie H, Kang YJ. Role of copper in angiogenesis and its medicinal implications. Curr. Med. Chem.. 16(10):1304–1314.
[16] Z. Chen, H. Meng, G. Xing, C. Chen, Y. Zhao, G. Jia, et al., Acute toxicological effects of copper nanoparticles in vivo, Toxicol. Lett. 163 (2) (2006 May 25) 109–120.
[17] L. Liverani, T. Reiter, K. Zheng, Z. Neščáková, A.R. Boccaccini, Copper-doped cotton-like malleable electrospun bioactive glass fibers for wound healing applications, Mater. Lett. X 14 (2022).
[18] E. Piatti, E. Verné, M. Miola, Synthesis and characterization of sol-gel bioactive glass nanoparticles doped with boron and copper, Ceram. Int. 48 (10) (2022) 13706–13718.
[19] S. Akhtach, Z. Tabia, K. El Mabrouk, M. Bricha, R. Belkhou, A comprehensive study on copper incorporated bio-glass matrix for its potential antimicrobial applications, Ceram. Int. 47 (1) (2021) 424–433.
[20] S. Kapoor, D. Brazete, I.C. Pereira, G. Bhatia, M. Kaur, L.F. Santos, et al., Impact of transition metal ions on the structure and bioactivity of alkali-free bioactive glasses, J. Non-Cryst. Solids 506 (2019 Feb 15) 98–108.
[21] A. Mishra, L. Petit, M. Pihl, M. Andersson, T. Salminen, J. Rocherullé, et al., Thermal, structural and in vitro dissolution of antimicrobial copper-doped and slow resorbable iron-doped phosphate glasses, J. Mater. Sci. 52 (15) (2017 Aug 1) 8957–8972.
[22] C. Stähli, M. Shah Mohammadi, K.E. Waters, S.N. Nazhat, Characterization of aqueous interactions of copper-doped phosphate-based glasses by vapour sorption, Acta Biomater. 10 (7) (2014) 3317–3326.
[23] K. Schuhladen, X. Wang, L. Hupa, A.R. Boccaccini, Dissolution of borate and borosilicate bioactive glasses and the influence of ion (Zn, Cu) doping in different solutions, J. Non-Cryst. Solids 502 (2018 Dec 15) 22–34.
[24] J. Han, N. Hassani Besheli, D. Deng, B.A.J.A. Van Oirschot, S.C.G. Leeuwenburgh, F. Yang, Tailoring copper-doped bioactive glass/chitosan coatings with angiogenic and antibacterial properties, Tissue Eng. C Methods 28 (7) (2022) 314–324.
[25] H. Zhu, M. Monavari, K. Zheng, T. Distler, L. Ouyang, S. Heid, et al., 3D bioprinting of multifunctional dynamic nanocomposite bioinks incorporating Cu-doped mesoporous bioactive glass nanoparticles for bone tissue engineering, Small 18 (12) (2022).
[26] M. Miola, A. Cochis, A. Kumar, C.R. Arciola, L. Rimondini, E. Verné, Copper-doped bioactive glass as filler for PMMA-based bone cements: morphological, mechanical, reactivity, and preliminary antibacterial characterization, Materials 11 (6) (2018 Jun) 961.
[27] L.R. Rivera, A. Cochis, S. Biser, E. Canciani, S. Ferraris, L. Rimondini, et al., Antibacterial, pro-angiogenic and pro-osteointegrative zein-bioactive glass/copper

based coatings for implantable stainless steel aimed at bone healing, Bioact. Mater. 6 (5) (2021) 1479–1490.
[28] E. Borsella, A. Dal Vecchio, M.A. Garcia, C. Sada, F. Gonella, R. Polloni, et al., Copper doping of silicate glasses by the ion-exchange technique: a photoluminescence spectroscopy study, J. Appl. Phys. 91 (1) (2002 Jan) 90–98.
[29] S. Sakka, K. Kamiya, K. Kato, Incorporation of copper into glass by the Cu-Na ion exchange, J. Non-Cryst. Solids 52 (1) (1982 Dec 1) 77–90.
[30] D. Guldiren, S. Aydın, Antimicrobial property of silver, silver-zinc and silver-copper incorporated soda lime glass prepared by ion exchange, Mater. Sci. Eng. C 78 (2017 Sep 1) 826–832.
[31] M. Miola, E. Verné, Bioactive and antibacterial glass powders doped with copper by ion-exchange in aqueous solutions, in: Materials [Internet], 2016. May 24[cited 2020 Sep 15];9(6), https://www.ncbi.nlm.nih.gov/pmc/articles/PMC5456756/.
[32] M. Miola, E. Bertone, E. Vernè, In situ chemical and physical reduction of copper on bioactive glass surface, Appl. Surf. Sci. 495 (2019 Mar 30), 143559.
[33] A. Cochis, B. Azzimonti, C. Della Valle, E. De Giglio, N. Bloise, L. Visai, et al., The effect of silver or gallium doped titanium against the multidrug resistant Acinetobacter baumannii, Biomaterials 80 (2016 Feb 1) 80–95.
[34] T. Kokubo, H. Takadama, How useful is SBF in predicting in vivo bone bioactivity? Biomaterials 27 (15) (2006 May 1) 2907–2915.
[35] K. Rajamäki, T. Nordström, K. Nurmi, K.E.O. Åkerman, P.T. Kovanen, K. Öörni, et al., Extracellular acidosis is a novel danger signal alerting innate immunity via the NLRP3 inflammasome, J. Biol. Chem. 288 (19) (2013 May 10) 13410–13419.
[36] L. Bingel, D. Groh, N. Karpukhina, D.S. Brauer, Influence of dissolution medium pH on ion release and apatite formation of Bioglass® 45S5, Mater. Lett. 143 (2015 Mar 15) 279–282.
[37] Thomas Luxbacher, The Zeta Guide - Principles of the Streaming Potential Technique, first ed., Anton Paar GmbH, Graz, Austria, 2014, p. 137.
[38] R. Sorrentino, A. Cochis, B. Azzimonti, C. Caravaca, J. Chevalier, M. Kuntz, et al., Reduced bacterial adhesion on ceramics used for arthroplasty applications, J. Eur. Ceram. Soc. 38 (3) (2018 Mar 1) 963–970.
[39] A. Cochis, J. Barberi, S. Ferraris, M. Miola, L. Rimondini, E. Vernè, et al., Competitive surface colonization of antibacterial and bioactive materials doped with strontium and/or silver ions, Nanomaterials 10 (1) (2020 Jan) 120.
[40] S. Ferraris, A. Cochis, M. Cazzola, M. Tortello, A. Scalia, S. Spriano, et al., Cytocompatible and anti-bacterial adhesion nanotextured titanium oxide layer on titanium surfaces for dental and orthopedic implants, in: Front Bioeng Biotechnol [Internet], 2019 [cited 2020 Sep 24];7. Available from: https://www.frontiersin.org/articles/10.3389/fbioe.2019.00103/full.
[41] International Standard Organisation (Iso), in: ISO 22196:2011 Measurement of Antibacterial Activity on Plastics and Other Non-porous Surfaces, 2011.
[42] G. Vourlias, Application of X-rays diffraction for identifying thin oxide surface layers on zinc coatings, Coatings 10 (10) (2020 Oct) 1005.
[43] K. Zheng, X. Dai, M. Lu, N. Hüser, N. Taccardi, Boccaccini AldoR, Synthesis of copper-containing bioactive glass nanoparticles using a modified Stöber method for biomedical applications, Colloids Surf. B Biointerfaces 150 (2017 Feb 1) 159–167.
[44] H. Wang, S. Zhao, W. Xiao, J. Xue, Y. Shen, J. Zhou, et al., Influence of Cu doping in borosilicate bioactive glass and the properties of its derived scaffolds, Mater. Sci. Eng. C 58 (2016 Jan 1) 194–203.
[45] V.S. Stoll, J.S. Blanchard, [4] buffers: principles and practice, in: M.P. Deutscher (Ed.), Methods in Enzymology [Internet], vol. 182, Academic Press, 1990 [cited 2023 Oct 20]. pp. 24–38. (Guide to Protein Purification;, https://www.sciencedirect.com/science/article/pii/007668799082006N.
[46] A. Ressler, A. Žužić, I. Ivanišević, N. Kamboj, H. Ivanković, Ionic substituted hydroxyapatite for bone regeneration applications: a review, Open Ceram 6 (2021 Jun 1), 100122.
[47] N.V. Bulina, N.V. Eremina, O.B. Vinokurova, A.V. Ishchenko, M.V. Chaikina, Diffusion of copper ions in the lattice of substituted hydroxyapatite during heat treatment, Materials 15 (16) (2022 Jan) 5759.
[48] M. Blochberger, L. Hupa, D.S. Brauer, Influence of zinc and magnesium substitution on ion release from Bioglass 45S5 at physiological and acidic pH, in: Biomed Glas [Internet], 2015. Sep 14[cited 2023 Mar 20];1(1), https://www.degruyter.com/document/doi/10.1515/bglass-2015-0009/html.
[49] S. Ferraris, S. Yamaguchi, N. Barbani, M. Cazzola, C. Cristallini, M. Miola, et al., Bioactive materials: in vitro investigation of different mechanisms of hydroxyapatite precipitation, Acta Biomater. 102 (2020 Jan 15) 468–480.
[50] S. Ferraris, S. Yamaguchi, N. Barbani, C. Cristallini, G. Gautier di Confiengo, J. Barberi, et al., The mechanical and chemical stability of the interfaces in bioactive materials: the substrate-bioactive surface layer and hydroxyapatite-bioactive surface layer interfaces, Mater. Sci. Eng. C 116 (2020 Mar 1), 111238.
[51] C.M. Botelho, M.A. Lopes, I.R. Gibson, S.M. Best, J.D. Santos, Structural analysis of Si-substituted hydroxyapatite: zeta potential and X-ray photoelectron spectroscopy, J. Mater. Sci. Mater. Med. 13 (12) (2002 Dec 1) 1123–1127.
[52] C. Pierre, G. Bertrand, I. Pavy, O. Benhamou, C. Rey, C. Roques, et al., Antibacterial electrodeposited copper-doped calcium phosphate coatings for dental implants, J. Funct. Biomater. 14 (1) (2023 Jan) 20.
[53] R.A. Popescu, K. Magyari, A. Vulpoi, D.L. Trandafir, E. Licarete, M. Todea, et al., Bioactive and biocompatible copper containing glass-ceramics with remarkable antibacterial properties and high cell viability designed for future in vivo trials, Biomater. Sci. 4 (8) (2016 Jul 19) 1252–1265.
[54] F. Foroutan, J. McGuire, P. Gupta, A. Nikolaou, B.A. Kyffin, N.L. Kelly, et al., Antibacterial copper-doped calcium phosphate glasses for bone tissue regeneration, ACS Biomater. Sci. Eng. 5 (11) (2019 Nov 11) 6054–6062.
[55] R. Koohkan, T. Hooshmand, M. Tahriri, D. Mohebbi-Kalhori, Synthesis, characterization and in vitro bioactivity of mesoporous copper silicate bioactive glasses, Ceram. Int. 44 (2) (2018 Feb 1) 2390–2399.
[56] M. Lallukka, A. Houaoui, M. Miola, S. Miettinen, J. Massera, E. Verné, In vitro cytocompatibility of antibacterial silver and copper-doped bioactive glasses, in: Ceram Int [Internet], 2023. Aug 31[cited 2023 Sep 13], https://www.sciencedirect.com/science/article/pii/S0272884223025518.